Mineralogy and Petrology (2004) 81: 265–278
DOI 10.1007/s00710-004-0037-5

Mineralogy and Petrology

The low-boron contest: minimising surface contamination and analysing boron concentrations at the ng/g-level by secondary ion mass spectrometry

H. R. Marschall and **T. Ludwig**

Mineralogisches Institut, Universität Heidelberg, INF 236, Heidelberg, Germany

Received October 3, 2003; accepted February 2, 2004
Editorial handling: A. Beran and E. Libowitzky

Summary

In-situ analyses of boron using secondary ion mass spectrometry (SIMS) is impeded by surface contamination of the analysed samples. We analysed 40 different natural and synthetic silicate materials, including meteoritic and mantle minerals, in order to find a material with an extremely low boron content that allows us to quantify the level of contamination. Different cleaning procedures were tested, and it was shown that using an ultrasonic cleaner with ultrapure water to clean the sample and setting the imaged field of the ion probe smaller than the primary beam spot reduces the boron contamination level to <2 ng/g at a total analysis time of $\sim$12 min (pre-sputtering: 400 s).

Herasil 102, a pure synthetic SiO_2 glass manufactured by Heraeus Quarzglas GmbH, Germany, was found to contain ≤ 1 ng/g boron, and therefore we recommend this glass as a sample to test the contamination level of boron in SIMS analyses.

Results for lithium show that analysis of this element is also influenced by contamination, but the contamination levels are much lower than those for boron.

Introduction

Boron has become a useful chemical tracer in both terrestrial and extraterrestrial materials. Despite its growing importance there is still a very restricted number of publications concerning boron in the Earth's mantle or in meteorites. This can be ascribed to the fact that samples – like polished thin sections – are always contaminated with boron on the surface, in cracks and at grain boundaries (*Shaw* et al.,

1988a). This was recognised early (*Anders* and *Ebihara*, 1982) and an approximate level of contamination is given in every publication dealing with boron at low concentrations (<10 µg/g). These levels depend on the techniques of sample preparation and cleaning procedures. Using the SIMS technique, they can vary between 10–50 ng/g (*Chaussidon* et al., 1997) and 2–5 µg/g (*Domanik* et al., 1993). Recent studies on meteoritic samples report lower contamination levels of 10 ng/g (*Kent* and *Rossman*, 2002) or below 10 ng/g (*Sugiura* et al., 2001). Ottolini (pers. communication, 2003) reported a contamination level of 5 ng/g in peridotite minerals during SIMS analysis. However, a unified method for sample preparation and analyses of boron at low concentrations is still lacking. This has serious implications for the quality of the data, because concentrations of boron in most mantle rocks and meteorites are lower than 1 µg/g (*Shaw* et al., 1988b; *Chaussidon* and *Libourel*, 1993). The scope of this work is to compare different analytical setups of SIMS, to present a method to reliably suppress boron contamination and analyse boron concentrations down to the ng/g-level. Furthermore, we wanted to find a silicate material containing ideally no boron at all in order to check the maximum level of contamination.

Surface contamination and its recognition in SIMS analysis

Dynamic SIMS is a method where material is removed from the sample's surface (typical erosion rates: 30 nm/h–10 µm/h). With a perfectly homogenous and well-defined primary beam at an incidence angle of 0° the surface contamination would not contribute to the analytical result once the contamination layer was removed. In reality, the beam current density distribution is not homogeneous, the beam is not perfectly spacially confined, it carries a (hopefully weak) halo of poorly focused neutrals and the incidence angle is >0°. Therefore the bottom of the sputtered crater is not flat, its edge is not perfectly steep and the surface contamination at the crater's edge continues to contribute to the result of the analysis (see Fig. 1).

A complete analysis with SIMS usually comprises several acquisition cycles. In each cycle, all unknown isotope(s) (e.g. ^{11}B) and the internal reference isotope (e.g. ^{30}Si) are analysed. Concentrations of the unknown element(s) are calculated

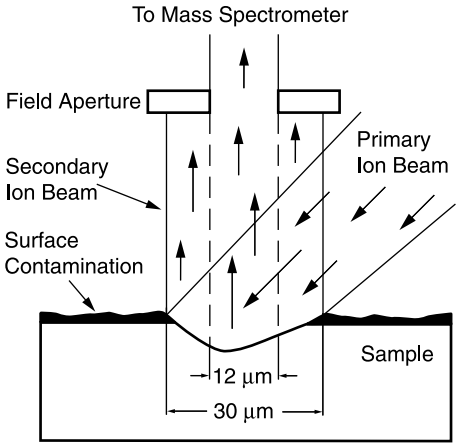

Fig. 1. Schematic drawing of the sputtering process. The pure sample (white) is covered with a contamination layer (black). Although most of the contamination is removed during the analysis, there is always some contamination present at the rim of the crater, which will be suppressed by field aperture FA2 (12 µm imaged field). Please note that this is a simplified drawing and that the real layout is more complex

by averaging the results of all measurement cycles, while the (relative) standard deviation of the mean is a measure for the precision of the analysis. Measurements influenced by surface contamination show decreasing unknown-to-reference ratios (or apparent element concentrations) in the course of the analysis. In case of contamination these ratios can decrease by more than one order of magnitude within the first 100 s. This has already been recognised by other authors for B, K and Na (*Sugiura* et al., 2001; *Müller* et al., 2003) as an indication of contamination, prohibiting a quantification of these trace elements at low concentration levels.

Quantitative analysis of trace elements with SIMS is usually done with an electron multiplier detector working in a pulse counting mode. In this mode at low concentrations (low count rates), where other sources of random error such as primary beam instability or instability of the magnet of the mass spectrometer are negligible, the precision of the result will be dominated by the counting statistics of the trace element.

For the average unknown-to-reference ratio Poisson statistics predict a relative standard error $(1RSD_{\text{mean}})$ of $1/\sqrt{N}$, where N is the total number of trace element ions counted. While a stable signal related to the true sample concentration will give a standard error close to $1/\sqrt{N}$, the decreasing count rates of an element in case of contamination will give a $1RSD_{\text{mean}} \gg 1/\sqrt{N}$. Thus a much higher standard error than predicted may be used as an indication of surface contamination.

Another method of recognising contamination is by analysing the same sample with a varying primary beam current I_{p}. Given the primary beam is always focused, a lower beam current results in a smaller spot. Moreover, since the contribution of the contaminated crater's edge to the total flow of secondary ions increases with a decreasing spot size, the apparent concentration will rise with a falling primary current when contamination is predominant. On clean samples (relative to the trace element concentration), the measured concentration will be independent from I_{p}.

The third method of evaluating the contamination level is measuring a sample containing extremely low concentrations (ideally zero) of the element of interest, which will be more sensitive towards contamination. The widely used NIST SRM glasses are not suitable for this purpose, as the concentration of boron in SRM 616, nominally containing the lowest trace element concentrations (200 ng/g) of all SRM 61x glasses, is still too high.

Reduction of contamination in sample preparation and of its effect during analysis

Lubricants and cooling liquids ordinarily used in saws and polishing machines for preparation of thin sections may contain several percent of boric acid. These liquids were replaced by pure glycol in our preparation lab. Prior to SIMS analyses, the samples are coated with carbon and investigated by electron microprobe. After microprobe analyses the carbon coating is removed with γ-alumina powder and distilled water. In order to remove boron contamination from the surface and cracks, the samples are first cleaned with acetone, then with distilled water (simple cleaning) and eventually in an ultrasonic cleaner using ultrapure water from a Milli-Q water purification system (Millipore). Ultrasonic cleaning with fresh ultrapure water is performed twice for $\sim$15 min (ultrapure cleaning).

In a simplified model, the contaminated sample may be considered a pure sample covered with a contamination layer. Analysing the pure sample then requires acquiring a depth profile. In depth-profiling, it is common practice to mechanically limit the secondary beam in order to overcome the described negative effects of the crater edge (*Benninghoven* et al., 1987) as shown schematically in Fig. 1. Using an imaged field smaller than the spot size, secondary ions coming from the edge of the crater will be suppressed. On Cameca ims 3(4, 5, 6)f instruments this is accomplished by selecting a field aperture of appropriate size in combination with the magnification factor of the selected transfer lens. Typically, depth profiling is performed by scanning the primary beam over an area much larger than the area covered by the imaged field, but this reduces the effective count rates and thus rises the detection limit. Therefore we chose a setup where the imaged field is only slightly smaller (factor $\sim$0.5) than the primary beam spot, which also allows us to analyse with a lateral resolution $\sim$30 µm. While a small field aperture has the advantage of reducing the contamination signal it also has some disadvantages: the count rate will be lower, resulting in a higher detection limit and the reproducibility will be worse because the beam has to be perfectly centred with respect to the field aperture for each analysis. At low concentration levels both disadvantages are outweighed by the reduced influence of surface contamination. The field aperture was not found to influence significantly the relative ion yield (RIY) of boron, which was 0.55 ± 0.01 for $^{11}B/^{30}Si$.

Analytical setup

The boron concentrations presented in Table 1 were measured by secondary ion mass spectrometry (SIMS) with a modified Cameca ims 3f ion microprobe (equipped with a primary beam mass filter) at Heidelberg. Analyses were performed using a 14.5 keV/20 nA $^{16}O^-$ primary ion beam with a diameter of $\sim$30 µm. Positive secondary ions were accelerated to a nominal energy of 4.5 keV. The energy window of the mass spectrometer was set to 40 eV and we employed the energy filtering technique with an offset of 75 eV at a mass resolution $m/\Delta m$ (10%) of $\sim$1000 to suppress interfering molecules and to minimise matrix effects (*Ottolini* et al., 1993). The ims 3f has three field apertures to limit the field imaged by the secondary beam. The influence of contamination was reduced by using the intermediate field aperture FA2 (750 µm) which reduces the imaged field to $\sim$12 µm in the 25 µm imaged field mode. Secondary ion intensities of ^{11}B were normalised to the count rate of ^{30}Si and calibrated against the NIST SRM 610 standard reference material (356.4 µg/g boron; *Pearce* et al., 1997) for all silicates. One analysis comprised 10 cycles with an integration time of 16 s/cycle for boron. Pre-sputtering on every spot lasted $\sim$6 min and analysis took another 4 min, resulting in $\sim$10 min total analysis time. The background of the mass spectrometer and the counting system near mass 11 u was determined in several analyses with an integration time of 1500 s each (50 cycles; 30 s/cycle) at mass 10.8 u with the same setup and Herasil 102 as sample. The background count rate was 0.021 cps and was subtracted from the boron count rates for each cycle of an analysis prior to calculating the mean value and the standard error.

Table 1. *Samples investigated with SiO_2 content and measured boron concentrations*

Sample	Type	Rock	Locality/Origin	Chemistry	SiO_2 (wt %)	B (ng/g)	2 RSD_{mean} (%)
Meteoritic and mantle minerals							
RFX1	Forsterite	CV3 meteorite	Allende	Mg_2SiO_4	42.8	**2.6**	208
B5	Olivine	Lherzolite	Eifel/D	$(Mg,Fe)_2SiO_4$	41.2	**83.3**	19.8
	Amphibole			Mg-Hastingsite	43.3	**157**	20.2
	Enstatite			$(Mg,Fe)SiO_3$	56.5	**78.3**	14.1
	Diopside			$Ca(Mg,Fe)Si_2O_6$	52.8	**114**	13.3
31-C	Enstatite	Harzburgite	Jizan/SA	$(Mg,Fe)SiO_3$	56.7	**3.6**	127
	Olivine			$(Mg,Fe)_2SiO_4$	41.2	**7.8**	83.3
1960/5 [1]	Pyrope	Grt-Lherzolite	Marsabit/K	$(Mg,Ca,Fe)_3Al_2Si_3O_{12}$	42.8	**6.9**	90.4
	Diopside			$Ca(Mg,Fe,Al)Si_2O_6$	53.6	**57.5**	39.9
	Olivine			$(Mg,Fe)_2SiO_4$	40.8	**44.0**	41.1
	Enstatite			$(Mg,Fe)SiO_3$	56.1	**50.7**	24.4
Ch-88-1[2]	Olivine	Dunite	Reunion/F	$(Mg,Fe)_2SiO_4$	38.9	**65.9**	34.0
ILR-84-4 [2]	Olivine	Dunite	Reunion/F	$(Mg,Fe)_2SiO_4$	40.5	**34.4**	29.7
Z31/1 [3]	Enstatite	Orthopyroxenite	Zabargad/EG	$(Mg,Fe,Al)SiO_3$	54.7	**97.5**	19.9
Z104 [3]	Olivine	Olivinite	Zabargad/EG	$(Mg,Fe)_2SiO_4$	41.5	**4708**	2.0
AA-3P5 [4]	Pyrope	Grt-Lherzolite	Alpe Arami/CH	$(Mg,Ca,Fe)_3Al_2Si_3O_{12}$	41.7	**7.8**	52.8
84-32	Enstatite	Spl-Lherzolite	Harrat Uwayrid/SA	$(Mg,Fe)SiO_3$	54.8	**14.3**	55.7
Magmatic minerals							
B3	Acmite	Phonolite	Gran Canaria/E	$NaFeSi_2O_6$	51.9	**1249**	2.3
B7	Olivine	Basaltic tuff	Hawai'i/USA	$(Mg,Fe)_2SiO_4$	40.9	**15.6**	69.2
B8	Olivine	Basalt	Hawai'i/USA	$(Mg,Fe)_2SiO_4$	40.8	**14.3**	59.2
Ro36 [5]	Enstatite	Norite	Romsaas/N	$(Mg,Fe)SiO_3$	55.3	**664**	8.4
B4 [6]	Beryl	Vein	Adun-Tschilon/RU	$Be_3Al_2Si_6O_{18}$	68.0	**117**	10.5
Metamorphic minerals							
30589-2 [7]	Kyanite	Granulite	Schwarzwald/D	Al_2SiO_5	37.2	**28.5**	52.1

(*continued*)

Table 1 (*continued*)

Sample	Type	Rock	Locality/Origin	Chemistry	SiO_2 (wt %)	B (ng/g)	2 RSD_{mean} (%)
	Almandine			$(Fe,Ca,Mg)_3Al_2Si_3O_{12}$	36.8	**37.2**	30.1
SA161	Quartz	Granulite	Granulitgebirge/D	SiO_2	100.0	**351**	10.0
	Almandine			$(Fe,Ca,Mg)_3Al_2Si_3O_{12}$	36.8	**96.6**	14.5
ZEH1 [8]	Quartz	Amphibolite	Schwarzwald/D	SiO_2	100.0	**206**	14.8
B2	Kyanite	Ky-Qtz vein	Prilep/MK	Al_2SiO_5	37.2	**17.1**	46.1
SY425D	Quartz	Omp-Qtz vein	Syros/GR	SiO_2	100.0	**20.3**	27.4
80-3 [9]	Quartz	Phe-Qtz vein	Trescolmen/CH	SiO_2	100.0	**191**	11.0
SY309A	Titanite	Blueschist	Syros/GR	$CaTiSiO_5$	30.2	**3.2**	171
SY304	Chloritoid	Blueschist	Syros/GR	$(Fe,Mg)_2Al_4Si_2O_{10}(OH)_4$	24.1	**6.4**	54.4
	Almandine			$(Fe,Ca,Mg)_3Al_2Si_3O_{12}$	37.0	**17.6**	41.7
B9	Quartz	Single crystal	Herkimer/USA	SiO_2	100.0	**2.1**	119
Synthetic materials							
B1C	Glass	Synth.	Min HD	Nd–Cr–Al–Si–O	27.5	**64.1**	28.8
B1D	Glass	Synth.	Min HD	Nd–Cr–Al–Si–O	27.3	**92.9**	27.0
RP1	Glass	Synth.	Min HD	Fe–Ca–Mg–Si–O	47.4	**5927**	2.0
B11	Forsterite	Synth.	Min HD	Mg_2SiO_4	43.5	**6.7**	79.0
Herasil 102	Glass	Synth.	Heraeus	SiO_2	100.0	**1.0**	212
W1	Glass	Synth.	–	SiO_2	100.0	**27.4**	28.9
W2	Glass	Synth.	–	SiO_2	100.0	**29.0**	15.8
HD2	Glass	Synth.	Min HD	Ca–Al–Ti–Si–O	37.5	**1252**	4.1

RSD_{mean} relative standard deviation of the mean. *Synth.* synthetic materials. *Min HD* synthesised at the Mineralogisches Institut Heidelberg. Localities: *D* Germany, *F* France, *GR* Greece, *SA* Saudi Arabia, *K* Kenya, *MK* Macedonia, *RU* Russia, *CH* Switzerland, *N* Norway, *E* Spain, *EG* Egypt. References for samples: [1] *Olker*, 2001, [2] *Staudacher* et al., 1990, [3] *Kurat* et al., 1993, [4] *Paquin* et al., 2004, [5] *Meyer*, 1989 [6] *Kirsten*, 1964, [7] *Marschall* et al., 2003, [8] *Hepp*, 2003, [9] *Zack* et al., 2002

Table 2. *Comparison of apparent boron concentrations in Herasil 102 for different virtual analytical setups and cleaning procedures. Data is extracted from the analyses shown in Fig. 3*

Shown in figure...	Cleaning procedure	Field aperture	Presputtering time (s)	No. of cycles	Integration time (s)	$^{11}B/^{30}Si$	Apparent conc. (ng/g)	2 RSD_{mean} (%)	x_C (x_D) (ng/g)
Virtual setup 1: Very short setup without presputtering (initial contamination)									
3a	simple	FA1	<10	1	30	1.8×10^{-4}	2283	–	1.6 (6.7)
3b	simple	FA2	<10	1	30	4.9×10^{-5}	635	–	6.0 (25)
3c	ultrapure	FA1	<10	1	30	8.2×10^{-5}	1053	–	1.6 (6.7)
3d	ultrapure	FA2	<10	1	30	1.9×10^{-5}	248	–	6.0 (25)
Virtual setup 2: Normal setup with presputtering for routine work									
3a	simple	FA1	400	10	300	6.7×10^{-7}	8.6	31.9	0.51 (1.4)
3b	simple	FA2	400	10	300	1.8×10^{-7}	2.4	96.5	1.9 (5.1)
3c	ultrapure	FA1	400	10	300	3.0×10^{-7}	3.9	28.7	0.51 (1.4)
3d	ultrapure	FA2	400	10	300	1.4×10^{-7}	1.7	102	1.9 (5.1)
Virtual setup 3: Setup with long presputtering and long integration time									
3a	simple	FA1	2000	50	1500	1.1×10^{-7}	1.4	26.4	0.23 (0.53)
3b	simple	FA2	2000	50	1500	1.2×10^{-7}	1.6	77.9	0.9 (2.0)
3c	ultrapure	FA1	2000	50	1500	8.0×10^{-8}	1.0	33.9	0.23 (0.53)
3d	ultrapure	FA2	2000	50	1500	8.4×10^{-8}	1.1	93.0	0.9 (2.0)

RSD_{mean} relative standard deviation of the mean, x_C critical level, x_D minimum detectable concentration

At 20 nA primary current and for the SRM 610, the setup described had an absolute boron sensitivity of 7.2 cps/(μg/g) and an apparent background concentration of 2.9 ng/g (Note that it does not make sense to define a sensitivity normalized to the primary current, because the secondary intensity does not increase further with increasing primary beam current once the primary beam spot is larger than the imaged field). The detection limit for boron is calculated using the ''working'' expressions for radioactivity from *Currie* (1968). For an integration time of 160 s the average background signal is $\mu_B = 160\,s \cdot 0.021cps = 3.36$ counts. Since the background signal was analysed separately, not in paired observations, the detection limits are calculated for a ''well-known'' blank. For the setup described, the critical value of the net signal is $S_C = 1.64\sqrt{\mu_B} \approx 3.0$ counts and the minimum detectable value is $S_D = 2.71 + 3.29\sqrt{\mu_B} \approx 8.7$ counts, hence for boron concentration the critical value x_C is 2.6 ng/g and the minimum detectable value x_D is 7.6 ng/g.

For the data presented in Fig. 3 and Table 2, some of the analyses were done with the large field aperture FA1 (1.8 mm), resulting in an imaged field of ~32 μm, and the same primary beam current (20 nA). Because of the larger field aperture this setup has a higher absolute boron sensitivity of 26.7 cps/(μg/g) and while the background count rate remains unchanged, the boron background concentration is lowered to 0.8 ng/g. The detection limits for these analyses are presented together with the data.

Experimental results and discussion

We collected a broad variety of 40 different natural and synthetic silicate materials in order to select a material that could be suitable to test the boron contamination level. All analyses were performed after applying the ultrapure cleaning procedure and using the field aperture FA2. The results of all samples are listed in Table 1. In some samples, less than 10 ng/g boron was measured and the lowest concentration obtained was 1.0 ng/g in the synthetic SiO_2 glass Herasil 102, which is well below the critical value x_D for the setup used. Uncertainties, given as relative 2-sigma standard deviation of the mean (standard error), are dominated by counting statistics. The high relative standard deviations (>100%) for concentrations <10 ng/g are due to the fact that the net boron signal was near or below the critical value S_C.

The relation between measured boron concentration and the relative standard error for all samples listed in Table 1 is plotted in Fig. 2. Note that here the data is *not* corrected for background, because the poisson statistics are valid for the gross signal including the background signal. Additionally, in Fig. 2 the predicted standard error, valid for an absolute boron sensitivity of 7.2 cps/(μg/g) and an integration time of 160 s, is plotted. The predicted and the actual standard errors are in good agreement, giving no indication of contamination. An example for analyses of a heavily contaminated sample is also shown in Fig. 2. For the analyses shown, this sample (Grt SY304) was not prepared using glycol, was not cleaned using the ultrapure procedure and the field aperture was FA1. For these analyses the predicted standard error is plotted as well. The difference between prediction and reality is obvious and provides a strong indication of contamination.

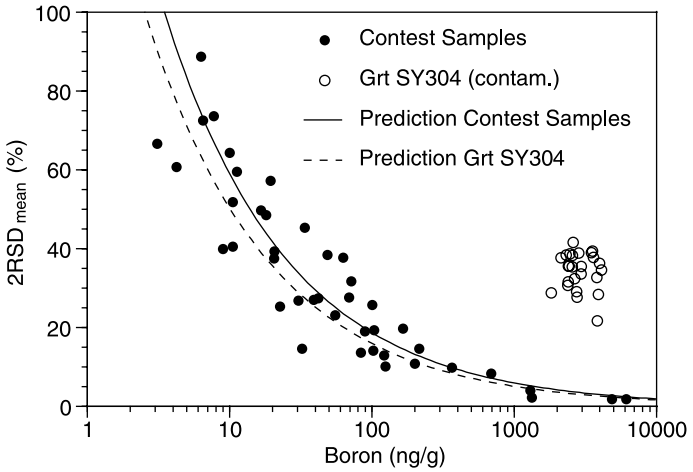

Fig. 2. Comparison of the relative standard error $2RSD_{\text{mean}}$ of real analyses (Contest Samples, Grt SY304) with the error predicted for the setups used. For the Contest Samples, predicted and measured error are in good agreement whereas for the contaminated sample SY304, the real error is much larger than the predicted

To check the efficacy of our analytical method with respect to B contamination, the sample with the lowest boron concentration (Herasil 102) was used. Analyses comprising 100 acquisition cycles with an integration time of 30 s for ^{11}B and 1 s for ^{30}Si per cycle were performed. Prior to each analysis the sample was sputtered for a few seconds – long enough to remove most of the gold layer and to achieve reasonably stable count rates for ^{30}Si. These measurements were performed with field apertures FA1 and FA2 before (simple cleaning) and after the sample was cleaned with ultrapure water (ultrapure cleaning). The results of these analyses are presented in Fig. 3, where the $^{11}B/^{30}Si$ ratio is plotted against sputtering time. It is evident that both the ultrapure cleaning and the use of field aperture FA2 make the B count rate decrease more rapidly towards the true value.

By extracting certain acquisition cycles (e.g. cycles No. 11 to 20), virtual analytical setups were simulated. These virtual analyses with their pre-sputtering times, integration times and detection limits x_C and x_D are presented in Table 2. The detection limits are calculated for the absolute sensitivities (depending on the field aperture chosen) as given in the analytical setup section and the integration time of each virtual setup.

Virtual setup 1 serves to demonstrate the initial level of boron contamination. Although Herasil 102 is a ''perfect'' sample (e.g., no pores, no cracks, no inclusions, size >1 mm, perfectly polished) the surface contamination leads to an apparent boron concentration of 2.3 μg/g for the simple cleaning procedure and 1.1 μg/g for the ultrapure cleaning procedure when analysed with field aperture FA1. Even without any pre-sputtering, the apparent boron concentrations are much lower with field aperture FA2, which proves the efficacy of our method. It is important to note that even a ''perfect'' sample surface is not safe from contamination.

Virtual setup 2 with a pre-sputtering time of 400 s and an integration time of 300 s represents a typical setup for routine analysis of low boron concentrations.

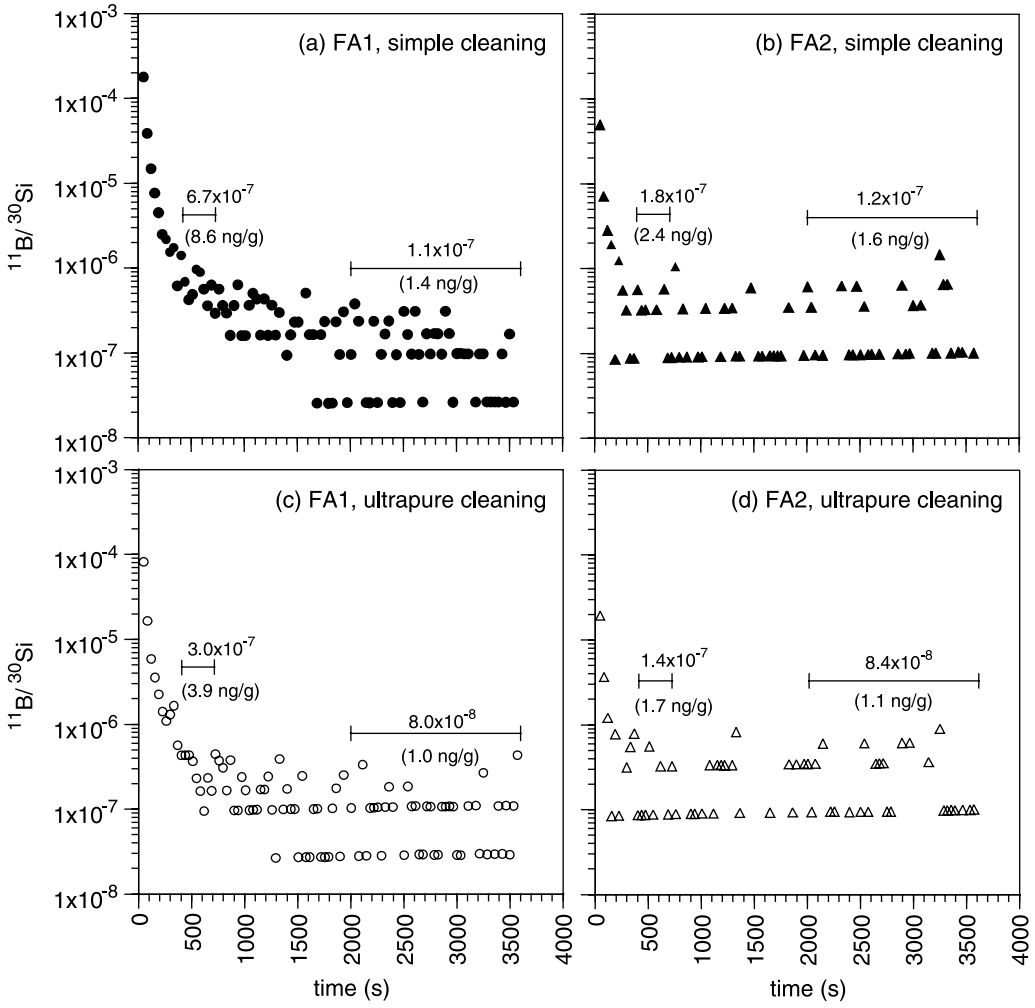

Fig. 3. Comparison of different analytical setups and cleaning procedures. **a** Imaged field 32 µm (FA1) and simple cleaning procedure, **b** imaged field 12 µm (FA2) and simple cleaning procedure, **c** imaged field 32 µm (FA1) and ultrapure cleaning procedure and **d** imaged field 12 µm (FA2) and ultrapure cleaning procedure. All diagrams show the $^{11}B/^{30}Si$ ratio as a function of sputtering time for the sample Herasil 102. The bars denote the results of the virtual setups described in the text and shown in Table 2

With simple cleaning and field aperture FA1 we get an apparent boron concentration of 8.6 ng/g, which is reduced to 3.9 ng/g by the ultrapure cleaning procedure and to 2.4 ng/g by applying the field aperture FA2. Combining both methods results in 1.7 ng/g in a total analysis time of ∼12 min per spot. The boron concentration of Herasil 102 is obviously below x_C and x_D of this virtual setup, which achieves a contamination level clearly below its detection limits.

Virtual setup 3 is a setup with a presputtering time of 2000 s, an integration time of 1500 s and a total analysis time of ∼1 h, resulting in very low detection limits. For this virtual setup the size of the field aperture does not make a significant difference, because after 2000 s the contaminated rim of the sputtered crater

has moved outside the imaged field of FA1 (32 µm). The ultrapure cleaning procedure still gives boron concentrations lower by ~0.5 ng/g. The measured concentration of ~1 ng/g is at or above the detection limits. This qualifies Herasil 102 as an excellent sample to test B contamination in SIMS analysis.

Implications for other elements

Our results and the results of other authors show that in-situ analysis of B is impeded by surface contamination, which makes it obligatory to use very elaborate cleaning procedures and analytical setups. This may not be restricted to boron, but is most likely also true for other trace elements. *Müller* et al. (2003) observed

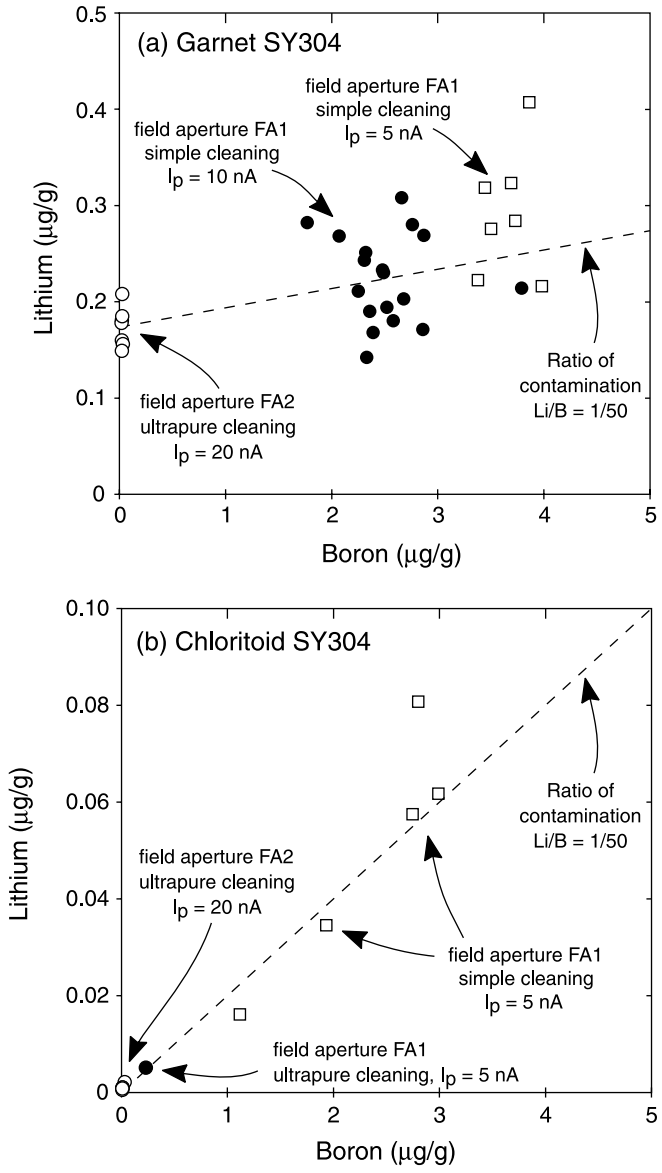

Fig. 4. Li vs. B concentrations of **a** garnet and **b** chloritoid in sample SY304, analysed with different setups and different cleaning procedures. The dotted line shows the approximate Li/B contamination ratio of 1/50 in both samples (note the different scales for Li). I_p primary beam current

surface contamination of Na, K and Fe during trace element analyses of quartz. During our study, we also measured Li and Be. Be did not show any sign of contamination and concentrations in some samples (Grt, Ol, Qtz) were less than 1 ng/g. Lithium, however, was found to be influenced by contamination. This was demonstrated for garnet and chloritoid in sample SY304, which were analysed with different primary beam currents, after different cleaning procedures and with field aperture FA1 as well as with FA2. The diagrams in Fig. 4 show that with field aperture FA1 and the simple cleaning procedure, the contamination of Li on the sample results in a contribution of contamination to the analysed value in the range of 20–200 ng/g. Cleaning the thin-section in the ultrasonic cleaner with ultrapure water reduces contamination level to ~5 ng/g. An average Li/B contamination ratio of ~1/50 can be calculated from both garnet and chloritoid in sample SY304. Therefore, in our lab, contamination is 50 times more significant for B than for Li.

Conclusions

Combining an efficient cleaning procedure with a very basic depth-profiling method enables us to reduce boron contamination to levels close to or even below the detection limit of ~2 ng/g (critical level x_C), with a lateral resolution of ~30 μm in a rather short time of ~12 min per spot. Other methods like pre-sputtering or scanning a larger area prior to analysis may reduce contamination to a level of ~10 ng/g (*Kent* and *Rossman*, 2002), but require more time and suffer from poor lateral resolution.

The SiO_2 glass Herasil 102 from Heraeus Quarzglas GmbH, Germany, is an appropriate material for checking the level of boron contamination of an in-situ analytical method like SIMS. Herasil 102 is an ultrapure, homogeneous material that is available in large quantities. A small sample of Herasil 102 can also be requested from the authors.

Natural minerals, like olivine, ortho- and clinopyroxene, garnet and quartz are not viable for testing the contamination level, as boron abundances in these minerals vary significantly among different samples and often reach levels of >100 ng/g.

Results for Li, B, Na, K and Fe (this study and *Müller* et al., 2003) suggest that contamination is a serious problem during in-situ analysis of various trace elements and must be controlled during analysis of materials showing very low concentrations, such as quartz, mantle rocks and meteorites. Contamination of boron, however, is much more significant than e.g. Li contamination.

Acknowledgements

The collection of all samples presented in this work was part of a ''Low-Boron Contest'' at our Institute. We are grateful to all participants of the contest for providing silicate materials: *R. Altherr, R. Bernhard, M. Bornefeld, M. Ebert, A. Helbling, S. Hepp, D. Hezel, J. Hopp, M. Kaliwoda, S. Klemme, E. W. Lowe, H. P. Meyer, J. Ogiermann, B. Olker, J. Paquin, G. Partzsch, S. Prowatke, M. Trieloff* and *T. Zack*. Heraeus Quarzglas kindly provided the Herasil 102 glass sample. We thank *R. Altherr, T. Zack* and *S. Prowatke* for fruitful discussions and *E. W. Lowe* for improving the English style. *B. Lefevre* and *L. Ottolini* are thanked for comments

that helped to improve the manuscript. This study was first presented at the LERM symposium in Nové Mesto, Czech Republic in June 2003. Financial support for this work was provided by the Deutsche Forschungsgemeinschaft (grants KA 1023/8-1 and AL 166/15-3).

References

Anders E, Ebihara M (1982) Solar-system abundances of the elements. Geochim Cosmochim Acta 46: 2363–2380

Benninghoven A, Rüdenauer FG, Werner HW (1987) Secondary ion mass spectrometry. John Wiley & Sons, New York Chichester Brisbane Toronto Singapore

Chaussidon M, Libourel G (1993) Boron partitioning in the upper mantle: an experimental and ion microprobe study. Geochim Cosmochim Acta 57: 5053–5062

Chaussidon M, Robert F, Mangin D, Hanon P, Rose EF (1997) Analytical procedures for the measurement of boron isotope composition by ion microprobe in meteorites and mantle rocks. Geostand Newslett 21: 7–17

Currie LA (1968) Limits for qualitative detection and quantitative determination. Anal Chem 40: 586–593

Domanik K, Hervig RL, Peacock SM (1993) Beryllium and boron in subduction zone minerals: an ion microprobe study. Geochim Cosmochim Acta 57: 4997–5010

Hepp S (2003) Amphibolite als Dokumente orogener Prozesse – eine Fallstudie aus dem Schwarzwald (Mitteleuropäische Variszіden). Thesis, University of Heidelberg (unpublished)

Kent AJR, Rossman GR (2002) Hydrogen, lithium, and boron in mantle-derived olivine: the role of coupled substitutions. Am Mineral 87: 1432–1436

Kirsten T (1964) Edelgasisotope in irdischen Mineralen und Gesteinen. Thesis, University of Heidelberg (unpublished)

Kurat G, Palme H, Embey-Isztin A, Touret J, Ntaflos T, Spettel B, Brandstätter F, Palme C, Dreibus G, Prinz M (1993) Petrology and geochemistry of peridotites and associated vein rocks of Zabargad Island, Red Sea, Egypt. Mineral Petrol 48: 309–341

Marschall HR, Kalt A, Hanel M (2003) P-T evolution of a Variscan lower-crustal segment: a study of granulites from the Schwarzwald, Germany. J Petrol 44: 227–253

Meyer H-P (1989) Zur Petrologie von Orbiculiten. Thesis, University of Karlsruhe (unpublished)

Müller A, Wiedenbeck M, van der Kerkhof AM, Kronz A, Simon K (2003) Trace elements in quartz – a combined electron microprobe, secondary ion mass spectrometry, laser-ablation ICP-MS, and cathodoluminescence study. Eur J Mineral 15: 747–763

Olker B (2001) Entwicklung und Anwendung eines Computerprogramms zur numerischen Modellierung von Diffusionsprofilen in Mineralkörnern. Thesis, University of Heidelberg (unpublished)

Ottolini L, Bottazzi P, Vanucci R (1993) Quantification of lithium, beryllium, and boron in silicates by secondary ion mass spectrometry using conventional energy filtering. Anal Chem 65: 1961–1968

Paquin J, Altherr R, Ludwig T (2004) Li-Be-B systematics in the ultrahigh-pressure garnet peridotite from Alpe Arami (Central Swiss Alps): implications for slab-to-mantle transfer. Earth Planet Sci Lett 218: 507–519

Pearce NJG, Perkins WT, Westgate JA, Gorton MP, Jackson SE, Neal CR, Chenery SP (1997) A compilation of new and published major and trace element data for NIST SRM 610 and NIST SRM 612 glass reference materials. Geostand Newslett 21: 115–144

Shaw DM, Higgins MD, Truscott MG, Middleton TA (1988a) Boron contamination in polished thin sections of meteorites: implications for other trace-element studies by alpha-track image or ion microprobe. Am Mineral 73: 894–900

Shaw DM, Higgins MD, Hinton RW, Truscott MG, Middleton TA (1988b) Boron in chondritic meteorites. Geochim Cosmochim Acta 52: 2311–2319

Staudacher T, Sarda P, Allègre CJ (1990) Noble gases systematics of Réunion Island, Indian Ocean. Chem Geol 89: 1–17

Sugiura N, Shuzou Y, Ulyanov A (2001) Beryllium-boron and aluminium-magnesium chronology of calcium-aluminium-rich inclusions in CV chondrites. Meteor Planet Sci 36: 1397–1408

Zack T, Foley SF, Rivers T (2002) Equilibrium and disequilibrium trace element partitioning in hydrous eclogites (Trescolmen, Central Alps). J Petrol 43: 1947–1974

Authors' address: *H. Marschall* (e-mail: hmarscha@min.uni-heidelberg.de) and *T. Ludwig* (e-mail: thomas.ludwig@min.uni-heidelberg.de), Universität Heidelberg, Mineralogisches Institut, Im Neuenheimer Feld 236, D-69120 Heidelberg, Germany